A Simplified Power Control Approach with Reliable Axis Decoupling Capability for Three-Phase Current Source Inverter

Amir Moghadasi, *Member, IEEE,* Arman Sargolzaei, *Member, IEEE,* Masood Moghaddami, *Student Member, IEEE,* Aditya Sundararajan, *Student Member, IEEE,* Arif Sarwat, *Member, IEEE,* and Kang Yen, *Senior Member, IEEE*

***Abstract*—This paper discusses the integration of a three-phase Distributed generation (DG) into a grid-tied Photovoltaic (PV) system. A single-stage power conversion system comprising a Current Source Inverter (CSI) capable of dc voltage boost is proposed for this PV MIC system, to control which, a multivariable−proportional−integral (PI) regulator-based power control strategy is designed. It will control the proposed CSI-based MIC system through structural simplicity and fast dynamic response. When contrasted with the conventional PI methods, the proposed control scheme grants a fully decoupled axes in terms of step jumps and falls in the active and reactive power commands. By controlling the modulation index and the angle introduced by the Phasor PWM (PPWM) switching patterns, the active and reactive powers are demonstrated to be obtained and exchanged between the PV MIC and the grid. An experimental verification is provided to justify the performance of the proposed control method through a 300-VA laboratory prototype, and the results are compared with that of the conventional PI regulation approaches.**

***Index Terms*—Active and reactive power control, current source inverter (CSI), distributed generation (DG), phasor pulse-width modulation (PPWM), proportional-integral (PI) regulators.**

I. Introduction

DRAMATIC increase in the Renewable Energy Sources (RESs)-based Distributed Genertion (DG) systems has been observed during the very recent times [1]. To this effect, a great concern for the operation of grid-tied PV systems is on the rise. In order to interface these DGs with the existing power grid, power electronic devices such as inverters are primarily used. These power inverters come equipped with current control and synchronization schemes to ensure power exchange between the primary source and the grid such that the grid codes and standards like CSA-C22.2, UL 1741, IEEE 1547, and IEC 62109-1 are neither compromised nor violated [2].

When it comes to the interfacing units, the Voltage Source Inverters (VSIs) are the most commonly used in grid-connected RES-based DG scenarios, owing to their widespread availability and simplicity. In order to ensure a sustaining match with the utility-operated grid voltage, the VSI topologies usually require either a step-up transformer or a dc-dc converter, both of which are additional conversion stages, in order to boost the low input voltage to a higher output voltage. However, this additional step comes at the expense of bulkier size, reduced efficiency and greater cost [3], [4].

Single-stage Current Source Inverters (CSIs), on the other hand, have seldom been studied for such scenarios considering their low power ranges [5]–[8]. When looked at the comparative study between VSI and CSI presented in [9], it can be observed that the CSI is capable of offering a higher reliability at nearly the same efficiency as that provided by the VSI. The following can be considered to be the primary reasons to regard the single-stage CSIs, already a go-to technology for AC motor-drive industries, the best alternative topology for DG-integration application [10]: 1) CSI reduces the circuitry complexity and the overall system losses owing to its inherent dc voltage boost capabilities, 2) CSI delivers a smooth dc-side current that is a much sought after feature for intermittent sources, 3) A considerable reduction in cost and conduction losses have recently been achieved by the development of Reverse-Blocking (RB) IGBT switches that remove the series diodes from the CSI topology, and 4) CSI offers an additional short-circuit protection as compared to VSI due to the controlled dc current.

Selected Harmonic Elimination (SHE) and Space Vector PWM (SVPWM) switching patterns are two operation modes for a CSI [11]–[14]. owever, the boost ratio, which can be defined as V_m/V_{dc} (where V_m and V_{dc} are the magnitude of the phase voltage and dc-side voltage, respectively), is below 1.0 for SHE- and slightly above 1.0 for SVPWM-based CSIs. Recently, a switching technique formulated based on the voltage phasor quantities, termed as the Phasor PWM (PPWM) was proposed by [8], where the boost ratio in the PPWM-based CSI could easily be higher than 3.00, while the Total Harmonic Distortions (THD) is maintained below 5%. In contrast with other modulation schemes, more control flexibility and better dynamic performance is delivered by PPWM. A requirement for the DGs to be equipped with real-time active and reactive power control features is expected under the assumption of a widespread use of three-phase RES-based DG systems. Regulating the injected current into the grid, the active and reactive power values exchanged between the DG and the grid can be independently controlled.

The current regulation of the two-stage VSI-based MIC systems have been the focus of the previously documented control schemes. They are primarily centered on the concept of the dq rotating synchronous reference frame with the conventional linear Proportional−Integral (PI) regulators and the PWM technique. Originally proposed in [15], the PI-based current regulation approach was since extensively studied and adopted for the current control of both single as well as three-phase systems across various applications [5]–[7], [10], [11]. In the design of the PI controller, two distinct d- and q-

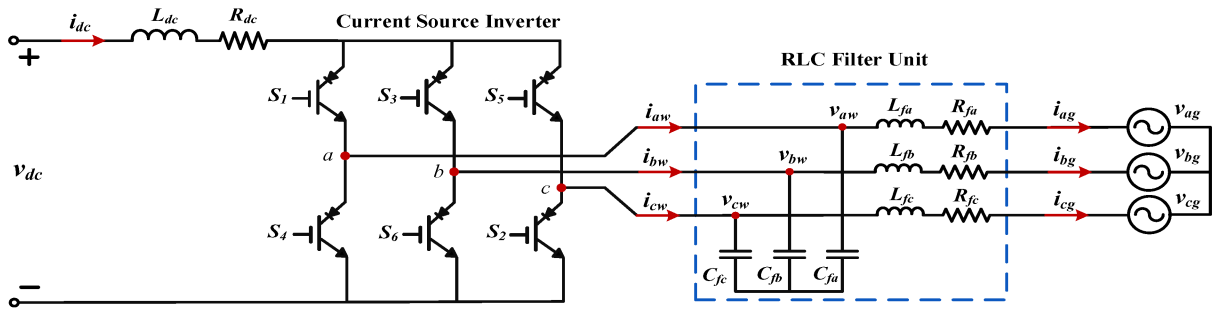

Fig. 1. Three-phase single-stage grid-connected CSI topology.

axis currents must be extracted in order to be independently regulated. However, due to the poor disturbance rejection capabilities, the d and q axes are not fully decoupled, and the step changes in one axis generate transients in the other, which might lead to power quality and performance deterioration. A multivariable PI controller with a faster dynamic response and superior axis decoupling capacity was proposed and experimentally evaluated for a three-phase VSI, in order to completely decouple d- and q-axis currents [16].

To the best knowledge of the authors, there have been no reports until this point in time, which fully consider the active and reactive power control of a CSI-based MIC system using a multivariable PI-based controller. Therefore, a multivariable PI current regulator for a three-phase single-stage grid-tied CSI topology is developed and proposed in this paper to bridge this gap. As the first step, a switching pattern based on PPWM technique is used to introduce modulation index and modulation angle, thereby generating switching signals. Secondly, a large-signal model is derived using the state-space averaging method with a combination of the dq reference frame. The procedure for control design corresponding to the multivariable PI regulator is illustrated, in which the active and reactive powers are almost fully decoupled so that the step changes in one power reference value negligibly affect the other. Next, an experimental evaluation of the proposed controller for a 300-VA laboratory prototype is conducted. Finally, the performance of the proposed scheme is compared with that of the conventional current regulation approach.

II. Configuration and Modulation Strategy

Figure 1 depicts the system architecture of the PV system, which uses a three-phase grid-tied CSI topology. The CSI circuit includes of a bridge with six reverse blocking (RB)-IGBT switches ($S_1 - S_6$) and a dc-link inductor L_{dc} as the main energy storage component with small resistance R_{dc}. RB-IGBTs are used as controllable switches for unidirectional current flow with reverse-blocking capability [17]. RB-IGBTs have a higher efficiency than a combination of an IGBT series with a diode that is typically used in CSIs. The system is connected to the three-phase grid voltages v_{ag}, v_{bg}, v_{cg} through the RLC filter unit, which smooths out the pulsed phase currents from the dc link. The voltages v_{aw}, v_{bw}, v_{cw} and currents i_{aw}, i_{bw}, i_{cw} represent the output voltages and currents of the inverter, as shown in Fig. 1.

Six sectors separated by six line-to-line voltage phasors exist, based on the PPWM modulation strategy [8], namely, V_{ab}, V_{bc}, V_{ca}, V_{ba}, V_{cb}, and V_{ac}, according to the zero-crossing points of grid voltages. Each of these sector is performed by three operating modes with switching cycle T_s, which includes three time intervals: t_c is the time interval for charging the dc-link inductor, and t_{d1} and t_{d2} are the time intervals for the discharging of the injection of the current to the CSI output terminals, and $T_s = t_c + t_{d1} + t_{d2}$. At any instant, there are only two active conducting switches, one from the upper (RB)-IGBTs (S_1, S_3, S_5) and one from the lower (RB)-IGBTs (S_4, S_6, S_2), to form a flow pass for the inductor current, i_{dc}.

If the voltage $V_{ab} = \sqrt{3}V_m \cos(\omega t)$ is considered as the reference signal, the charging and discharging intervals for all six sectors are considered as below [3]:

$$\begin{cases} t_{d1} = m_i T_s \cos(\omega t - \alpha_0) \\ t_{d2} = m_i T_s \cos(\omega t - \alpha_0 - \frac{2\pi}{3}) \\ t_c = T_s - (t_{d1} + t_{d2}). \end{cases} \tag{1}$$

where $0 < m_i \leq 1$ is the modulation index that can be utilized to adjust the level of dc current at the dc-link inductor, and modulation angle α_0 is the phase shift with respect to the voltage v_{ab} that can be applied to control the power factor of the CSI. The modulation index m_i can be obtained with respect to modulation angle α_0 as

$$m_i = \frac{2V_{dc}}{3V_m \cos(\alpha_0 + \pi/6)} \tag{2}$$

where V_m and V_{dc} are the magnitude of the phase voltage and dc-side voltage, respectively.

III. State-Space Average Modeling of CSI

The circuit diagrams, corresponding to the three possible switching states of the grid-tied CSI for Sector I, are shown in Fig. 2. In these state-space representations, the state vector x consists of state variables of the system, i.e., $x = [i_{dc} \;\; i_{ag} \;\; i_{bg} \;\; v_{ab}^w \;\; v_{bc}^w]^T$. Applying the periodic averaging technique [18] to these model results in state-space model $\dot{x} = A_I x + Bu$ for Sector I, where u is the input vector $u = [v_{dc} \;\; v_{ab}^g \;\; v_{bc}^g]^T$. The average state matrix of Sector I can be obtained from $A_I = [d_c A_c + d_1 A_{d1} + d_2 A_{d2}]$, where $d_c = t_c/T_s$, $d_1 = t_{d1}/T_s$, and $d_2 = t_{d2}/T_s$ are the corresponding duty ratios [19]. Similarly, the averaged system matrices for other sectors, A_{II}, A_{III}, A_{IV}, A_V, and A_{VI} can be obtained from their six sectors of PPWM and corresponding circuit diagrams, respectively.

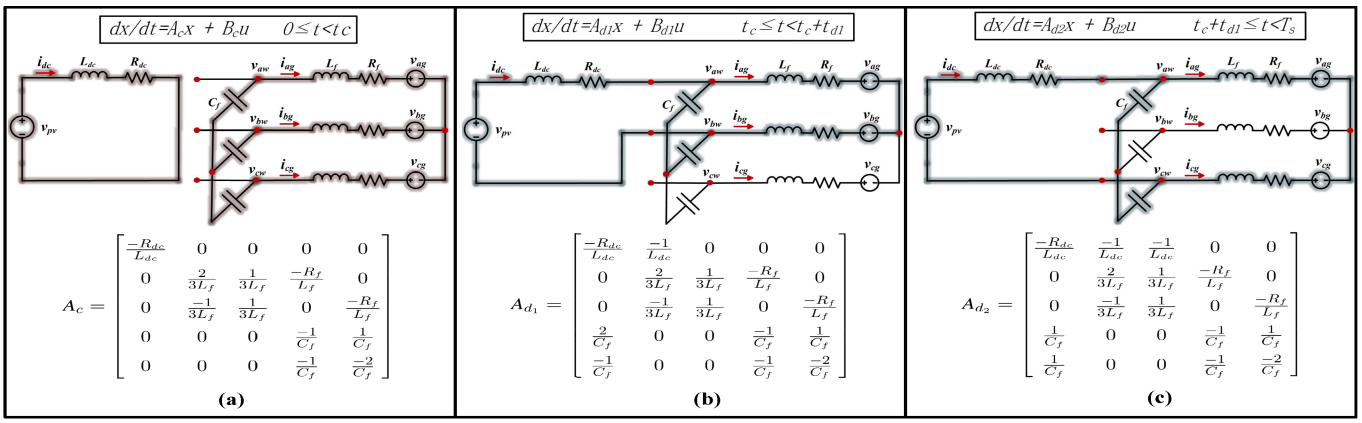

Fig. 2. Voltage and current of the dc-link inductor over one T_s in a CSI, while V_1 and V_2 are line-line voltage output.

A time invariant state-space averaging model is obtained by transferring the six state space representations to the synchronously rotating dq reference frame. The averaged matrices obtained for the six sectors in the dq reference frame can be proved to be equal to one another, i.e., $A_{dqI} = A_{dqII} = \cdots = A_{dqVI} = A_{dq}$, in which the A_{dq} represents the dynamic matrix of the large-signal model [19]. By virtue of this, the state-space average representation of the three-phase grid-tied CSI-based DG system in the rotating dq-frame of reference can be mathematically written as:

$$\frac{d}{dt}\begin{bmatrix} i_{dc} \\ i_{dg} \\ i_{qg} \\ v_{dw} \\ v_{qw} \end{bmatrix} = \underbrace{\begin{bmatrix} \frac{-R_{dc}}{L_{dc}} & 0 & 0 & \frac{-\alpha}{2L_{dc}} & \frac{-\beta}{2L_{dc}} \\ 0 & \frac{-R_f}{L_f} & \omega & \frac{1}{2L_f} & \frac{\sqrt{3}}{6L_f} \\ 0 & -\omega & \frac{-R_f}{L_f} & \frac{-\sqrt{3}}{6L_f} & \frac{1}{2L_f} \\ \frac{\alpha}{C_f} & \frac{-3}{2C_f} & \frac{\sqrt{3}}{2C_f} & 0 & \omega \\ \frac{\beta}{C_f} & \frac{-\sqrt{3}}{2C_f} & \frac{-3}{2C_f} & -\omega & 0 \end{bmatrix}}_{A_{dq}} \begin{bmatrix} i_{dc} \\ i_{dg} \\ i_{qg} \\ v_{dw} \\ v_{qw} \end{bmatrix} + \underbrace{\begin{bmatrix} \frac{1}{L_{dc}} & 0 & 0 \\ 0 & \frac{-1}{2L_f} & \frac{-\sqrt{3}}{6L_f} \\ 0 & \frac{\sqrt{3}}{6L_f} & \frac{-1}{2L_f} \\ 0 & 0 & 0 \\ 0 & 0 & 0 \end{bmatrix}}_{B} \begin{bmatrix} v_{pv} \\ v_{dg} \\ v_{qg} \end{bmatrix} \quad (3)$$

where $A = \sqrt{3}m_i \sin(\alpha_0)$ and $B = \sqrt{3}m_i \cos(\alpha_0)$. It should be noted that the input matrices are the same at any switching state, i.e., $B_c = B_{d1} = B_{d2} = B$ (see Fig. 2).

The 5th order state-space model shown in (3) can be used to study the stability and sensitivity of the three-phase grid-integrated CSI-based DG system. The design of a 300-VA laboratory prototype, whose parameters are tabulated in Table I, is proposed in this paper, wherein the modulations are set initial values of $m_i = 0.2$ and $\alpha_0 = -\pi/6$, and the grid voltage frequency is assumed fixed at $\omega = 120\pi$. The state vector at equilibrium ($X_{dq} = [61.46\ 0.48\ 12.16\ 34.82\ 148.57]^T$) is attained by substituting these values into (3). At the system operating point of about 300 W and 0 Var (RMS grid current of 0.86A), it designates the steady-state values of the state vector x_{dq}. The system's stability is signified by the non-positivity of the real components of all five eigenvalues, which are $\lambda_1 = -101.6$, $\lambda_{2,3} = -867.1 \pm j6065.9$, and $\lambda_{4,5} = -123.7 \pm j4718.3$. The variation of the dc-link voltage does not affect the proposed system's stability as a consequence of the system matrix in (3) being independent of v_{dc}.

TABLE I
CSI-BASED DG SYSTEM PARAMETERS

Parameters	Value	Parameters	Value
Rated power	300 VA	dc-link resistance	$R_{dc} = 0.2\ \Omega$
Rated phase voltage	120 V	dc-link inductance	$L_{dc} = 6\ mH$
Rated frequency	60 Hz	Filter capacitance	$C_f = 15\ \mu F$
Switching frequency	3 kHz	Filter inductance	$L_f = 2\ mH$
dc-link voltage	50 V	Filter resistance	$R_f = 2\ \Omega$

IV. PROPOSED POWER CONTROL SYSTEM

Reliable axis decoupling-equipped dq current controller for a modified PI is proposed, wherein the step changes in one axis negligibly affect the other. Gating signals are produced from charging and discharging intervals triggered by a PPWM switching pattern for CSI-based DG system. Modulation index m_i and modulation angle α_0 could be controlled to independently regulate active and reactive powers.

A. Comparative Study of Conventional and Developed PI−Based Current Control approach

Literature has plenty of sources on the conventional dq current control strategy [20]–[23]. Decoupled control of i_{dg} and i_{qg} can be achieved by controlling the output voltages of the converter, as shown below:

$$\begin{cases} v_{dw} = u_{cd} + 2R_f i_{dg} - 2L_f \omega i_{qg} + v_e \\ v_{qw} = u_{cq} + 2R_f i_{qg} + 2L_f \omega i_{dg} + v_f \end{cases} \quad (4)$$

where u_{cd} and u_{cq} are control signals in the d and q axes in the rotating reference frame, respectively, and the voltages $v_e = -\frac{\sqrt{3}}{3}v_{qw} + v_{dg} + \frac{\sqrt{3}}{3}v_{qg}$ and $v_f = \frac{\sqrt{3}}{3}v_{dw} + v_{qg} + \frac{\sqrt{3}}{3}v_{dg}$ are voltage feedforwards obtained from (3).

The structural diagram of the current regulator based on conventional PI controllers is illustrated by Fig. 3(a) in accordance with (4), wherein the voltage feedforwards and coupling

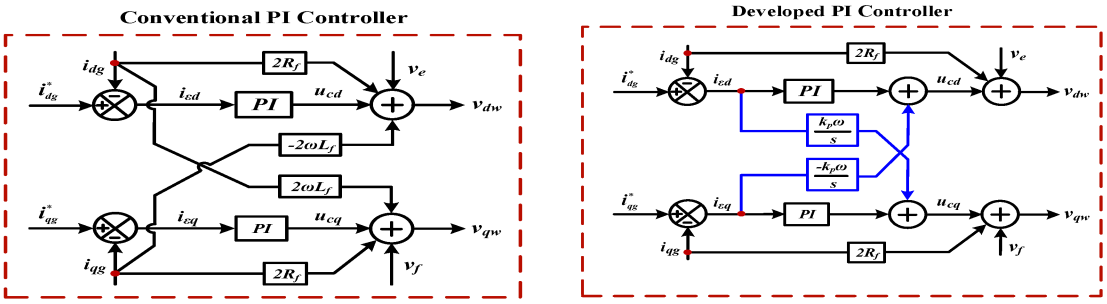

(a) (b)

Fig. 3. Structural diagram of dq current control. (a) Conventional PI-based controller. (b) Developed PI-based controller.

terms are depicted. A Laplace transformation $P(s)$ can be used to formulate the conventional PI controller:

$$P(s) = \frac{k_p s + k_I}{s}. \tag{5}$$

where, k_p and k_I are the proportional gain and integral gain of the controller, respectively.

It is noteworthy that adopting feedforward signals can theoretically create a fully decoupled system. However, complete decoupling can be achieved by using the feedforward signals to accurately neutralize the effect of nullifying the effect of the coupling terms ($\omega L_f i_{dg}$ and $\omega L_f i_{qg}$). Despite this possibility, the practicalness to precisely calculate the value of i_{dg}, i_{qg}, and L_f is infeasible given the errors in measurement on a real system. Moreover, an imperfect cancellation might take shape due to the delays induced by the sampling process. Therefore, in a practical sense, full decoupling of the axes cannot be achieved by implementing the conventional PI control strategy.

While the conventional PI-based control method relies on the feedforward signals to exclude coupling effects, the proposed PI-based technique employs the plant inversion approach to design a fully decoupled control system [16], [24]. It can, hence, be defined as

$$P(s) = \frac{[k_p(s + j\omega) + k_I]}{s}. \tag{6}$$

where the coupling between the d and q axes is denoted by term $j\omega k_p$. By separating the real and imaginary parts, the controller can be reformulated as

$$u_{cd} + j u_{cq} = (\frac{k_p s + k_I}{s} + j\frac{k_p \omega}{s})(i_{\varepsilon d} + j i_{\varepsilon q}) \tag{7}$$

where

$$u_{cd} = \frac{k_p s + k_I}{s} i_{\varepsilon d} - \frac{k_p \omega}{s} i_{\varepsilon q} \tag{8}$$

$$u_{cq} = \frac{k_p s + k_I}{s} i_{\varepsilon q} + \frac{k_p \omega}{s} i_{\varepsilon d} \tag{9}$$

where, $i_{\varepsilon d}$ and $i_{\varepsilon q}$ are the error signals of the d and q current axes in the rotating reference frame, respectively. The control signals in both the d and q axes are elborated in (8) and (9), including the cross-coupling terms. However, unlike the conventional PI controller, the coupling terms (i.e., $\frac{k_p \omega}{s} i_{\varepsilon q}$ and $\frac{k_p \omega}{s} i_{\varepsilon d}$) include integrators, which might significantly reduce the coupling effect of the axis on one another. Fig. 3(b) shows a structural diagram of the proposed PI controller resulting in a practically decoupled axis. The feedforward signals are adopted for cancelling the grid voltage disturbances.

B. Active and Reactive Power Control Implementation

Details of the proposed power control scheme for the three-phase grid-tied CSI-based DG system are depicted by Fig. 4. The major objectives for control objectives include: 1) tracking the reference dc-link current; 2) delivering a certain amount of active and reactive power; and 3) considerably decoupling the active and reactive powers from each other in response to the step changes in command signals. Two independent control loops for active and reactive powers respectively were combined to yield the controller. Three-phase grid currents i^g_{abc} are transformed into the dq components i_{dg} and i_{qg} in the grid-voltage reference frame in order to achieve independent control.

A synchronous angle is obtained through the grid-voltage Phase-Locked Loop (PLL). With the dq synchronous frame, the grid voltages v^g_{abc} only have the d-axis component v_{dg} while the q-axis component v_{qg} equals zero. Therefore, regulating the grid currents i_{dg} and i_{qg} can lead to the independent control of active and reactive powers from the DG to the grid, respectively, as shown below:

$$\begin{cases} P_g = 1.5 v_{dg} i_{dg} \\ Q_g = 1.5 v_{dg} i_{qg}. \end{cases} \tag{10}$$

By neglecting the loss in the system, the active power on the grid side is equal to the active power of the dc-link in a steady-state operation, which is given by

$$P_g = P_{CSI} = P_{dc} = V_{dc} I_{dc}. \tag{11}$$

where V_{dc} and I_{dc} are the dc-link voltage and current magnitude, respectively.

The PI controller with a control speed of T_s/L_{dc} is utilized to generate the d-axis reference of the grid current since the dc-link current is controlled in order for the CSI to supply the needed active power to the grid [5]. The error signal resulting from the comparison of the magnitude of the dc-link current reference I^*_{dc} determined from (11) with the measured dc-link current i_{dc} is fed into the PI regulator to produce a control signal of v^*_{Ldc}. The dc voltages of the PV side and converter side, along with the voltage across the dc-link inductance, satisfy the equation $v^*_{dc1} = V_{dc} - v^*_{Ldc}$. By neglecting the

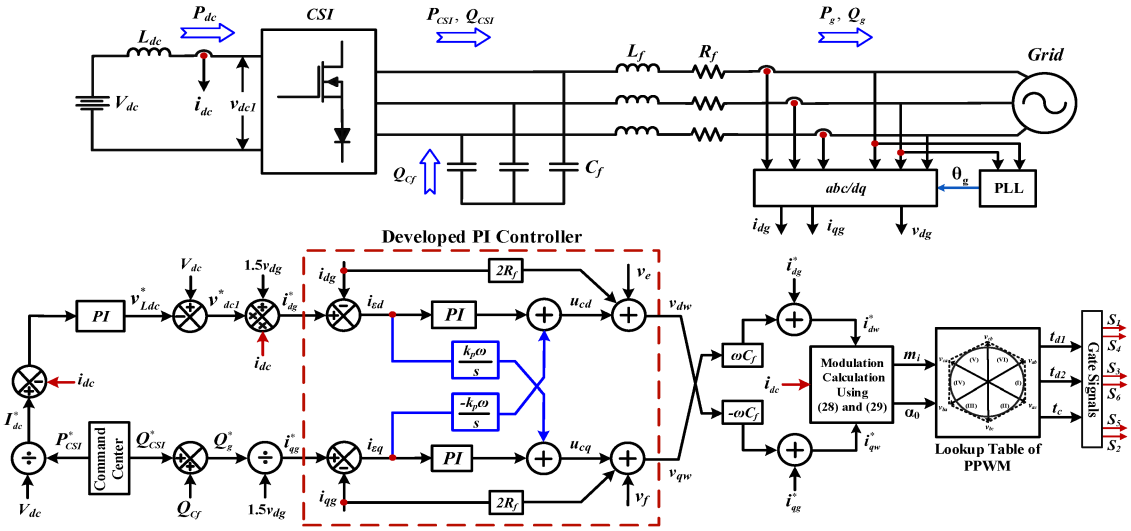

Fig. 4. Overall control block diagram of the three-phase grid-tied CSI-based DG system.

loss in the system, the grid reference current i_{dg}^* is derived based on the power-balance assumption, i.e.,

$$i_{dg}^* = \frac{P_g^*}{1.5v_{dg}} = \frac{v_{dc1}^* i_{dc}}{1.5v_{dg}}. \tag{12}$$

Proper control of the q-component current can help adjust the grid reactive power. In this study, a fixed amount of reactive power, Q_{C_f}, about 0.25 p.u. of the rated power, was injected by selecting a filter capacitor. The q-axis grid reference current i_{qg}^* was obtained by adding Q_{C_f} into the CSI reactive power command Q_{CSI}^* in order to find the total reactive power reference Q_g^* injected into the grid, as shown in (10).

The error signals obtained by comparing the measured active and reactive current signals, i_{dg} and i_{qg}, of the grid against their reference values are fed through the proposed PI controller with voltage feedforward in order to derive the converter output voltage values, as depicted in Fig. 3(b).

The steady-state dq components of the capacitor currents, derived by using converter output voltages, are $i_{dc_f} = -\omega C_f v_{qw}$ and $i_{qc_f} = \omega C_f v_{dw}$. Upon subtracting the capacitor current and the grid reference current, the output reference current provided by the converter is obtained, which can be written in the dq axes as:

$$\begin{cases} i_{dw}^* = i_{dg}^* - i_{dc_f} = i_{dg}^* + \omega C_f v_{qw} \\ i_{qw}^* = i_{qg}^* - i_{qc_f} = i_{qg}^* - \omega C_f v_{dw} \end{cases} \tag{13}$$

Finally, the currents of i_{dw}^* and i_{qw}^* are applied to (14) and (15) to produce the value of the modulation index m_i and the modulation angle α_0, namely control parameters as

$$m_i = \frac{\sqrt{{i_{dw}^*}^2 + {i_{qw}^*}^2}}{i_{dc}} \tag{14}$$

$$\alpha_0 = \arccos\left(\frac{2}{3m_i\beta}\right) - \frac{\pi}{6}. \tag{15}$$

The proposed system exploits the PPWM switching strategy in order to produce time intervals of charging and discharging for each sector using (1), i.e., t_c, t_{d1}, t_{d2}, so as to as finally achieve the control objectives defined earlier. However, it is to be noted that these time intervals must follow the angle $\theta_g = \omega t$.

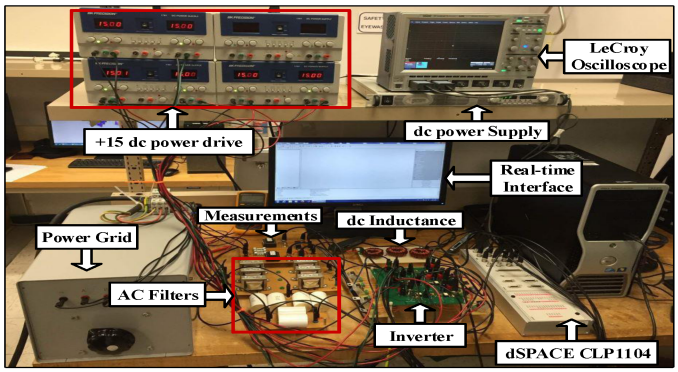

Fig. 5. Layout of the experimental setup.

V. Experimental Verification

A 300-VA grid-integrated prototype of three-phase, single-stage CSI was designed and built to evaluate the performance of the proposed multivariable PI-based power controller, which is illustrated by Fig. 5. Table I clearly tabulates the main system parameters which were used in the experimental work. A full-bridge inverter was constructed by RB-IGBTs, which their ratings are given in [25]. A 50 V power supply connected to the dc-link inductor with L_{dc}=6 mH and R_{dc}=0.2 Ω delivered the input voltage for this module. An RLC filter unit connects the inverter to the grid (3ph, 208 V line to line, 60 Hz), with the PPWM strategy applied to a switching frequency of 3kHz.

To meet the THD criteria recommended by IEEE STD 519-1992, the switching frequency was appropriately selected. It is noteworthy that the boost ratio in PPWM strategy was kept at about 3.4 ($\beta = V_m/V_{pv} = 170/50 = 3.4$). A dSPACE CLP1104 rapid prototype board was used to implement the proposed control scheme. The MATLAB/Simulink and dSPACE Control Desk were used together to apply signal processing algorithms. Upon applying a Particle Swarm Optimization (PSO) algorithm to the proposed system using MAT-

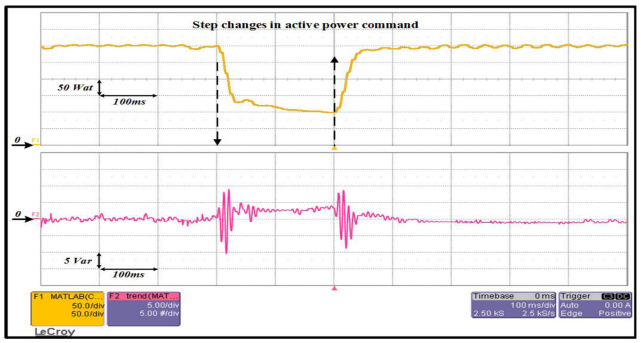

(a)

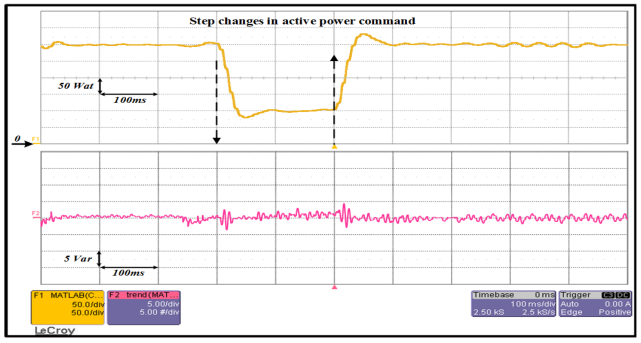

(b)

Fig. 6. Step changes in active power command. (a) Conventional PI-based controller. (b) Developed PI-based controller.

LAB/Simulink package in order to find the optimum values of the PI controllers to maintain the stability of the closed-loop control system, the PI controller for the dc-link current was set at k_p =0.005 and k_I =0.03, and the PI controller for power control was set at k_p =0.001 and k_I =0.15. The measurements were performed using a LeCroyWaverunner 64XI oscilloscope with a bandwidth of 600 MHz and carried out to demonstrate the performance of the proposed control system.

Keeping the reactive power command fixed, a step-down and step-up for the active power reference value of (P^*_{CSI}) was applied to demonstrate the dynamic response of the proposed control system. As exhibited by Fig. 6, two step changes in the reference value of the CSI's active power was used to experimentally evaluate the performance of the both control regulation scheems.

As a consequence of this, for this scenario, while the reference value for the reactive power was kept constant at $Q^*_{CSI} = 0$ during the entire process, the active power was initially considered to step-down from its rated value of 330 W to around 100 W, and after lapsing 0.2s, a step-up back to its rated value. The capability of the proposed PI-based controller to track the step-changes in the active power reference value, was nearly comparable to that of its traditional counterpart. This performance is further clarified by Figs. 6(a) and (b). Corresponding to the conventional PI controller (shown in Fig. 6(a)), the reactive power reference signal underwent non-negligible transients upon every step change. The transients verify that the d and q axes are not fully decoupled when the conventional PI-based control scheme was implemented for the CSI-based DG system. As depicted by Fig. 6(b), the developed PI controller reveals that for each step change in the active power command, the reference value of the reactive power, Q^*_{CSI}, withstands much lower amounts of transients.

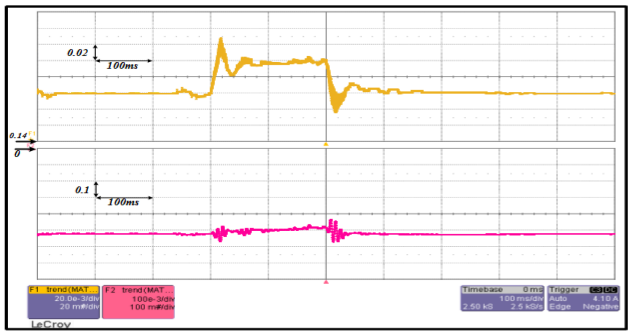

Fig. 7. Step changes in active power command. Description of plots: modulation index m_i on top and modulation angle α_0 on bottom.

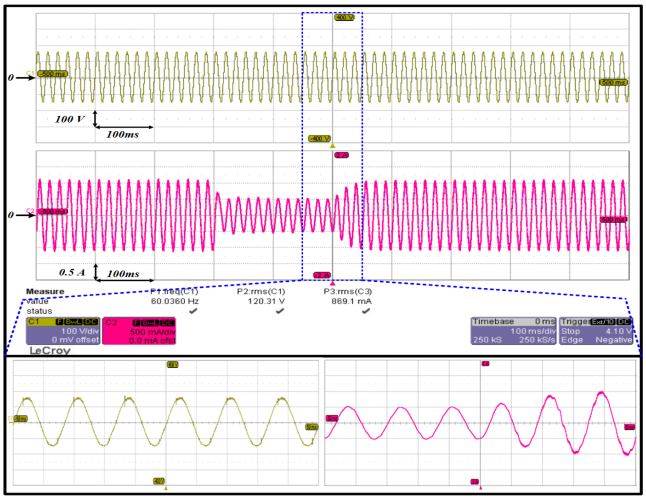

Fig. 8. Step changes in active power command. Description of plots: phase-a waveform of the grid voltage on top and grid current on bottom.

The modulation index, m_i, and the modulation angle, α_0, are controlled in order to deliver the active and reactive power exchanged between the grid and the DG system, as illustrated by the overall control block diagram shown in Fig. 4. To this effect, the value of m_i was changed from 0.2 to 0.22 in the step-down mode and brought back to the original value in the step-up mode and the value of α_0 was maintained at around its original value of -0.52 rad by the controller, as illustrated in Fig. 7. This in turn yields in an independent regulation of active and reactive power. A phase shift of $\pi/6$ rad between the CSI current phase angle φ_{inv} and modulation angle α_0 was noted based on (15), which could be correspondingly derived from $\varphi_{inv} = arctan(Q^*_{CSI}/P^*_{CSI})$ and $\alpha_0 = \varphi_{inv} - \pi/6$.

It was noted from Fig. 8 which shows the phase-a waveform of the grid voltage v_{ag} and the injected grid current i_{ag}, that the voltage remains unaffected during the step-changes while the magnitude and phase angle of the grid current alter corresponding to the reference value such that there is a steady state error. A fixed shift angle in the grid current was i_{ag} created with respect to v_{ag} upon injecting 25% of rated power (around 80 Var) by the selection of a filter capacitor, as stated in the previous section. The proposed PI controller delivers a reliable tracking response to regulate the active and reactive power. On another note, a step change of the CSI active power command causes the dc current to drop from 6A to around 2A,

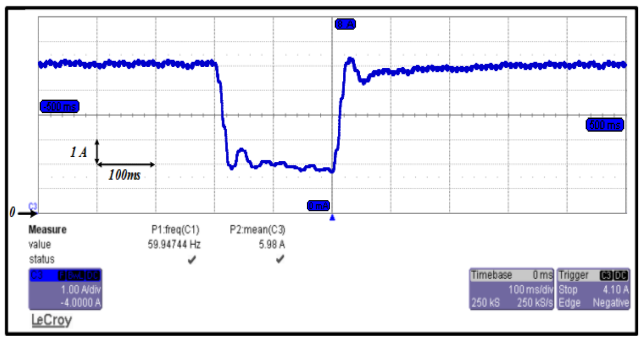

Fig. 9. Transient response of dc-link current during step changes in active power command.

as shown in Fig. 9.

VI. Conclusion

A 300-VA three-phase single-stage CSI was proposed and experimentally evaluated as a testbed for grid-tied PV systems. Aided by structural simplicity, a multivariable PI-based current control strategy was presented to independently control the active and reactive powers by regulating control parameters of m_i and α_0 , introduced by the PPWM switching patterns. Experimental results show that the proposed control system exhibits a promising dynamic response with respect to tracking the step changes in reactive and active power reference values. Moreover, the multivariable PI control method represents a superior axis decoupling capability, wherein the step changes in one power command signal negligibly affects the other. Open-loop eigenvalue analysis of the small signal model was utilized to study the dynamic behaviors of the three-phase grid-tied CSI-based DG system. In contrast to what was expected, it was concluded that the dc-link voltage had never affected the stability of the proposed system. The results also revealed the proposed system remained stable despite the control parameters of m_i and α_0 varying within the CSI's operating limits.

References

[1] T. Strasser, F. Andrn, J. Kathan, C. Cecati, C. Buccella, P. Siano, P. Leito, G. Zhabelova, V. Vyatkin, P. Vrba, and V. Mark, "A review of architectures and concepts for intelligence in future electric energy systems," *Industrial Electronics, IEEE Transactions on*, vol. 62, no. 4, pp. 2424–2438, April 2015.

[2] S. A. Khajehoddin, M. Karimi-Ghartemani, A. Bakhshai, and P. Jain, "A power control method with simple structure and fast dynamic response for single-phase grid-connected dg systems," *Power Electronics, IEEE Transactions on*, vol. 28, no. 1, pp. 221–233, Jan 2013.

[3] B. Mirafzal, M. Saghaleini, and A. Kaviani, "An SVPWM-based switching pattern for stand-alone and grid-connected three-phase single-stage boost inverters," *Power Electronics, IEEE Transactions on*, vol. 26, no. 4, pp. 1102–1111, April 2011.

[4] S. Liu, B. Ge, X. Jiang, H. Abu-Rub, and F. Z. Peng, "Comparative evaluation of three z-source/quasi-z-source indirect matrix converters," *Industrial Electronics, IEEE Transactions on*, vol. 62, no. 2, pp. 692–701, Feb 2015.

[5] B. Sahan, A. N. Vergara, N. Henze, A. Engler, and P. Zacharias, "A single-stage PV module integrated converter based on a low-power current-source inverter," *Industrial Electronics, IEEE Transactions on*, vol. 55, no. 7, pp. 2602–2609, July 2008.

[6] S. Anand, S. K. Gundlapalli, and B. G. Fernandes, "Transformer-less grid feeding current source inverter for solar photovoltaic system," *Industrial Electronics, IEEE Transactions on*, vol. 61, no. 10, pp. 5334–5344, Oct 2014.

[7] P. Cossutta, M. P. Aguirre, A. Cao, S. Raffo, and M. I. Valla, "Single-stage fuel cell to grid interface with multilevel current-source inverters," *Industrial Electronics, IEEE Transactions on*, vol. 62, no. 8, pp. 5256–5264, Aug 2015.

[8] A. Singh, A. Kaviani, and B. Mirafzal, "On dynamic models and stability analysis of three-phase phasor PWM-based CSI for stand-alone applications," *Industrial Electronics, IEEE Transactions on*, vol. 62, no. 5, pp. 2698–2707, May 2015.

[9] B. Sahan, S. V. Araujo, C. Noding, and P. Zacharias, "Comparative evaluation of three-phase current source inverters for grid interfacing of distributed and renewable energy systems," *Power Electronics, IEEE Transactions on*, vol. 26, no. 8, pp. 2304–2318, Aug 2011.

[10] A. A. A. Radwan and Y. A. R. I. Mohamed, "Analysis and active suppression of AC- and DC-side instabilities in grid-connected current-source converter-based photovoltaic system," *Sustainable Energy, IEEE Transactions on*, vol. 4, no. 3, pp. 630–642, July 2013.

[11] H.-J. Lee, S. Jung, and S.-K. Sul, "A current controller design for current source inverter-fed AC machine drive system," *Power Electronics, IEEE Transactions on*, vol. 28, no. 3, pp. 1366–1381, March 2013.

[12] M. Aguirre, L. Calvino, and M. Valla, "Multilevel current-source inverter with FPGA control," *Industrial Electronics, IEEE Transactions on*, vol. 60, no. 1, pp. 3–10, Jan 2013.

[13] Z. Bai, H. Ma, D. Xu, B. Wu, Y. Fang, and Y. Yao, "Resonance damping and harmonic suppression for grid-connected current-source converter," *Industrial Electronics, IEEE Transactions on*, vol. 61, no. 7, pp. 3146–3154, July 2014.

[14] R. Ni, Y. W. Li, Z. Cheng, and N. Zargari, "Virtual impedance based selective harmonic compensation (VI-SHC) PWM for current source rectifiers," in *Energy Conversion Congress and Exposition (ECCE), 2012 IEEE*, Sept 2012, pp. 1048–1055.

[15] C. Schauder and H. Mehta, "Vector analysis and control of advanced static var compensators," *Generation, Transmission and Distribution, IEE Proceedings C*, vol. 140, no. 4, pp. 299–306, Jul 1993.

[16] B. Bahrani, S. Kenzelmann, and A. Rufer, "Multivariable-PI-based dq current control of voltage source converters with superior axis decoupling capability," *Industrial Electronics, IEEE Transactions on*, vol. 58, no. 7, pp. 3016–3026, July 2011.

[17] H. Sarnago, O. Lucia, A. Mediano, and J. M. Burdio, "Modulation scheme for improved operation of an RB-IGBT-based resonant inverter applied to domestic induction heating," *Industrial Electronics, IEEE Transactions on*, vol. 60, no. 5, pp. 2066–2073, May 2013.

[18] J. A. Sanders and F. Verhulst, "Averaging methods in nonlinear dynamical systems," *New York, Springer-Verlag*, 1985.

[19] A. Kashefi Kaviani, "Dynamic modeling and analysis of single-stage boost inverters under normal and abnormal conditions," *FIU Electronic Theses and Dissertations*, 2012.

[20] H. Guzman, M. J. Duran, F. Barrero, L. Zarri, B. Bogado, I. G. Prieto, and M. R. Arahal, "Comparative study of predictive and resonant controllers in fault-tolerant five-phase induction motor drives," *Industrial Electronics, IEEE Transactions on*, vol. 63, no. 1, pp. 606–617, Jan 2016.

[21] N. Mukherjee and D. Strickland, "Control of cascaded dc-dc converter-based hybrid battery energy storage systems-;part i: Stability issue," *Industrial Electronics, IEEE Transactions on*, vol. 63, no. 4, pp. 2340–2349, April 2016.

[22] F. Freijedo, A. Vidal, A. Yepes, J. Guerrero, O. Lopez, J. Malvar, and J. Doval-Gandoy, "Tuning of synchronous-frame pi current controllers in grid-connected converters operating at a low sampling rate by MIMO root locus," *Industrial Electronics, IEEE Transactions on*, vol. 62, no. 8, pp. 5006–5017, Aug 2015.

[23] M. Farhadi and O. Mohammed, "Adaptive energy management in redundant hybrid dc microgrid for pulse load mitigation," *Smart Grid, IEEE Transactions on*, vol. 6, no. 1, pp. 54–62, Jan 2015.

[24] B. Widrow and E. Walach, "Adapting inverse control: A signal processing approach," *John Wiley*, 2008.

[25] IXRH25N120 RB-IGBT datasheet, "[online]. available: http://www.alldatasheet.com/datasheet-pdf/pdf/133079/IXYS/IXRH50N120.html."